Chemistry–A European Journal
Research Article
doi.org/10.1002/chem.202403676
Chemistry Europe
European Chemical Societies Publishing
www.chemeurj.org

Site-specifically Phosphorylated Hsp90C-terminal Domain Variants Provide Access to Deciphering the Chaperone Code.

Oliver Gajsek,[a, b] Christian F. W. Becker,*[a] and Anne C. Conibear*[c]

The ubiquitous molecular chaperone Heat shock protein 90 (Hsp90) is pivotal in many cellular processes through folding of client proteins under stressed and normal conditions. Despite intensive research on its function as a chaperone, the influence of posttranslational modifications on Hsp90 (the 'chaperone code'), and its interactions with co-chaperones and client proteins, still remains to be elucidated. The C-terminal domain (CTD) of Hsp90 is essential for formation of the active homodimer state of Hsp90 and contains recognition sites for co-chaperones and client proteins. Here we used expressed protein selenoester ligation to introduce site-selective phosphorylations in the Hsp90 CTD, while preserving the native amino acid sequence. The two phosphorylations do not affect the overall secondary structure, but in combination, slightly decrease the thermal stability of the CTD. The Hsp90 CTD functions as a chaperone in decreasing aggregation of model client proteins, but the C-terminal phosphorylations do not significantly alter the anti-aggregation activity for these clients. The optimization of expressed protein selenoester ligation (EPSL) to carry out several steps in one pot provides an efficient route to access site-specifically modified Hsp90 CTD variants, allowing the generation of Hsp90 variants with site-specific PTMs to decipher the chaperone code.

Introduction

The family of Heat shock proteins (Hsps) belongs to the class of molecular chaperones – proteins that interact with their substrates, often termed "clients", to facilitate their folding. This chaperone activity helps client proteins to acquire and/or maintain their native functionality under basal as well as stressed conditions.[1,2] Hsps are abundant and are expressed predominantly in the cytosol, but are found in all cellular compartments. When exposed to stressors such as heat, radiation, hypoxia or infection, eukaryotic cells increase the expression of Hsps as a defense mechanism that facilitates maintenance of homeostasis. Among the Hsps, Heat shock protein 90 (Hsp90, named after its ~90 kDa size) is one of the most abundant and has over 300 known client proteins,[3–5] including essential members of cellular signaling cascades, kinases, steroid hormone receptors, oncoproteins, and proteins involved in many neurodegenerative diseases.[6–9] The central role of Hsp90 in cellular homeostasis has made it for decades a target for new anticancer drugs that downregulate oncoprotein chaperoning;[10–12] however only recently an Hsp90 inhibitor received clinical approval for use against gastrointestinal stromal cancer.[11,13] The central role of Hsp90 in protein folding and homoeostasis makes it a promising but very challenging target, and emphasizes the need for a deep understanding of its molecular function and regulation.

In its active state, Hsp90 forms a homodimer in which each monomer consists of three conserved domains. The amino-terminal domain (NTD) contains the primary nucleotide (ATP) pocket and is linked *via* a highly charged and flexible linker sequence to the middle domain (MD), which provides a large surface area for client protein binding. The carboxy-terminal domain (CTD) initiates the dimer formation of Hsp90 and is therefore crucial for proper functioning of Hsp90.[5] The structured domains are flanked by intrinsically disordered linkers and tails. Initiated by the binding of ATP and the client protein, Hsp90 cycles through open and closed states, the 'chaperone cycle'; dimerization of the NTDs is followed by large conformational changes in the middle domain before the release of the properly folded and activated client, ADP and inorganic phosphate (Figure 1 a).[14–16] This cycle is regulated by a variety of co-chaperones that bind and dissociate Hsp90 and its clients to facilitate the chaperone activity. The Hsp90 CTD in isolation has also shown chaperone activity in a variety of model substrate aggregation assays. This anti-aggregation

[a] O. Gajsek, C. F. W. Becker
Institute of Biological Chemistry, Faculty of Chemistry, University of Vienna, Währingerstraße 39, 1090 Vienna, Austria
Phone: +43-1-4277-70501
E-mail: christian.becker@univie.ac.at
[b] O. Gajsek
University of Vienna, Vienna Doctoral School in Chemistry (DoSChem), Währinger Str. 42, 1090 Vienna, Austria
[c] A. C. Conibear
Institute of Applied Synthetic Chemistry, TU Wien, Getreidemarkt 9, 1060 Vienna, Austria
Phone: +43-1-58801-163723
E-mail: anne.conibear@tuwien.ac.at

Supporting information for this article is available on the WWW under https://doi.org/10.1002/chem.202403676

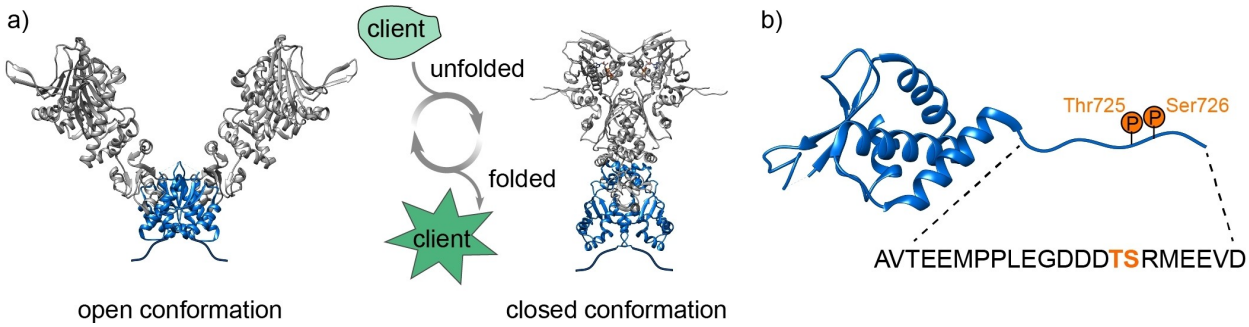

Figure 1. Structural and functional characteristics of Hsp90. a) Crystal structure of Hsp90 analogs in open (IPD:2IOQ) and closed conformational states (IDP: 2CG9). The intrinsically disordered C-terminal tail, residues ~700-732, is representationally added to the CTD (blue). During the chaperone cycle, Hsp90 undergoes large conformational changes upon binding of ATP and the client protein. This process is highly regulated by co-chaperones and posttranslational modifications. b) Domain structure of human Hsp90 alpha CTD (IPD:3Q6 N) with added C-terminal sequence, residues 711–732, containing the TPR recognition motif -MEEVD and two phosphorylations in proximity.

activity is dependent on dimer formation, which is mainly dependent on the CTD.[17–19] Furthermore, the intrinsically disordered C-terminal tail of the CTD is important for interacting with co-chaperones through a tetratricopeptide repeat (TPR) recognition site comprising the residues -MEEVD (Figure 1 b).[20–22]

The abundant posttranslational modifications (PTMs) of Hsp90 are thought to have a role in its selection of co-chaperones and client proteins under different conditions, and in different cellular locations. However, due to the large size of Hsp90, its many PTMs, and its multiple clients and co-chaperones, the so-called 'chaperone code' by which PTMs regulate the activity of Hsp90 is still largely undeciphered.[23–25] Homogeneous proteins bearing (multiple) native site-specific PTMs are usually only accessible by (semi−)synthesis strategies,[26,27] so previous studies have used natural amino acid mimics to study the impact of and crosstalk between PTMs of Hsp90. In a recent example, Mollapour and co-workers used non-phosphorylatable alanine or phosphomimetic glutamic acid mutants to study a phosphorylation site in yeast Hsp82 (Ser25, equivalent to human Hsp90α, Ser39), which is phosphorylated by autophagy activating kinase Atg1/ULK.[28] Mimetics of phosphorylation at this site caused inhibition of chaperone activity. Furthermore, phosphorylation of this site leads to dissociation of the Atg1/ULK12-Hsp90 complex, which allows Atg1/ULK1 to be activated and initiate autophagy. This regulation by a phosphorylation PTM showcases an intriguing interplay between Hsp90 and the serine/threonine kinase Atg1/ULK1, which itself is a client of Hsp90, and means that inhibition of Hsp90 leads to degradation of Atg1/ULK1.[29] A further example indicates the importance of PTMs close to the MEEVD TPR recognition site located in the C-terminal tail of the Hsp90 CTD; Gestwicki and co-workers studied the binding of TPR-domain-containing co-chaperones to Hsp70 and Hsp90 and found that mimicking phosphorylation of serine and threonine residues with glutamic acid near the -MEEVD motif selectively alters the binding to the TPR-domain-containing E3 ligase CHIP (Carboxy terminus of Hsp70-interacting protein), but not to other co-chaperones.[30] These examples highlight the potential pivotal insights that can be gained by a detailed study of the regulation of Hsp90 by PTMs. However, mutating phosphorylated serine or threonine residues to glutamic acid to mimic the charge and polarity of phosphorylation, does not always accurately mimic the behavior of phosphorylation PTMs,[31,32] so there is a need to access selectively modified Hsp90 variants.

Here we show a semi-synthesis strategy to access a set of four variants of the Hsp90 CTD to investigate the role of the C-terminal phosphorylation PTMs in the structure, biophysical properties, and chaperone activity of the Hsp90 CTD. We focus on adjacent phosphosites Thr725 and Ser726, within the C-terminal intrinsically disordered region of the Hsp90 CTD. These PTMs were identified in a curated database of the human phosphoproteome, in predictions, and in *in vitro* phosphorylation assays.[30,33] Although one phosphorylation is on threonine and the other on serine, their close proximity suggests that they might be installed by the same kinase that does not discriminate between the two sites. The presence of the doubly-phosphorylated variant would be difficult to detect in a complex cell lysate, but is theoretically possible and supported by predictions,[30] so was included in this study. Importantly, use of a diselenide-selenoester ligation[34,35] followed by deselenization allowed us to preserve the native amino acid sequence, including three native cysteine residues (Cys572, Cys597 and Cys598). The semi-synthesis route established in this work allows us to investigate the effects of PTMs in the Hsp90 CTD and provides a starting point for further semisynthetic access to site-selectively modified Hsp90 variants to decipher the chaperone code.

Results and Discussion

Optimization of an Efficient One-Pot Strategy to Access Site-Selectively Phosphorylated Hsp90 CTD

The location of the PTMs of interest, Thr725 and Ser726, in the C-terminus of the CTD suggests that site-specifically phosphorylated variants of the Hsp90 CTD could be readily accessed by an expressed protein ligation strategy, in which the recombinantly-expressed N-terminal segment would be ligated to a synthetic

(and phosphorylated) C-terminal segment.[36] However, this would require mutation to a cysteine or thiol-modified residue at the ligation site. This thiol ligation handle could be subsequently desulfurized,[37,38] but would involve concomitant desulfurization of the three native cysteine residues in the CTD (Cys572, Cys597 and Cys598). Based on the AlphaFold3-predicted structures and few available crystal structures (which all lack the C-terminal tail),[39–41] these cysteines are not close enough or suitably oriented to be involved in disulfide bonds with each other, but might be important for the folding and/or function of the Hsp90 CTD, for example in interactions with clients or co-chaperones, so desulfurizing them to alanine would be undesirable. We therefore devised a semi-synthesis strategy (Figure 2) that applies the recently-developed expressed protein selenoester ligation, in which a recombinant N-terminal segment bearing a C-terminal selenoester is ligated to the C-terminal synthetic segment bearing an N-terminal selenocysteine.[35] This allows for selective deselenization to the native alanine residue at the ligation site, while preserving the native cysteines.[42]

Using the site Ala710-Ala711 as a favorable ligation junction, the N-terminal recombinant segment (Hsp90_572-710) was designed as a C-terminally fused *Mxe*GyrA-His$_7$-CBD protein **1** and accessed *via* recombinant expression in *E. coli* (Figure 2b, Supplementary Figure S1). The N-terminal cysteine 572 at the junction between the CTD and middle domains also offers

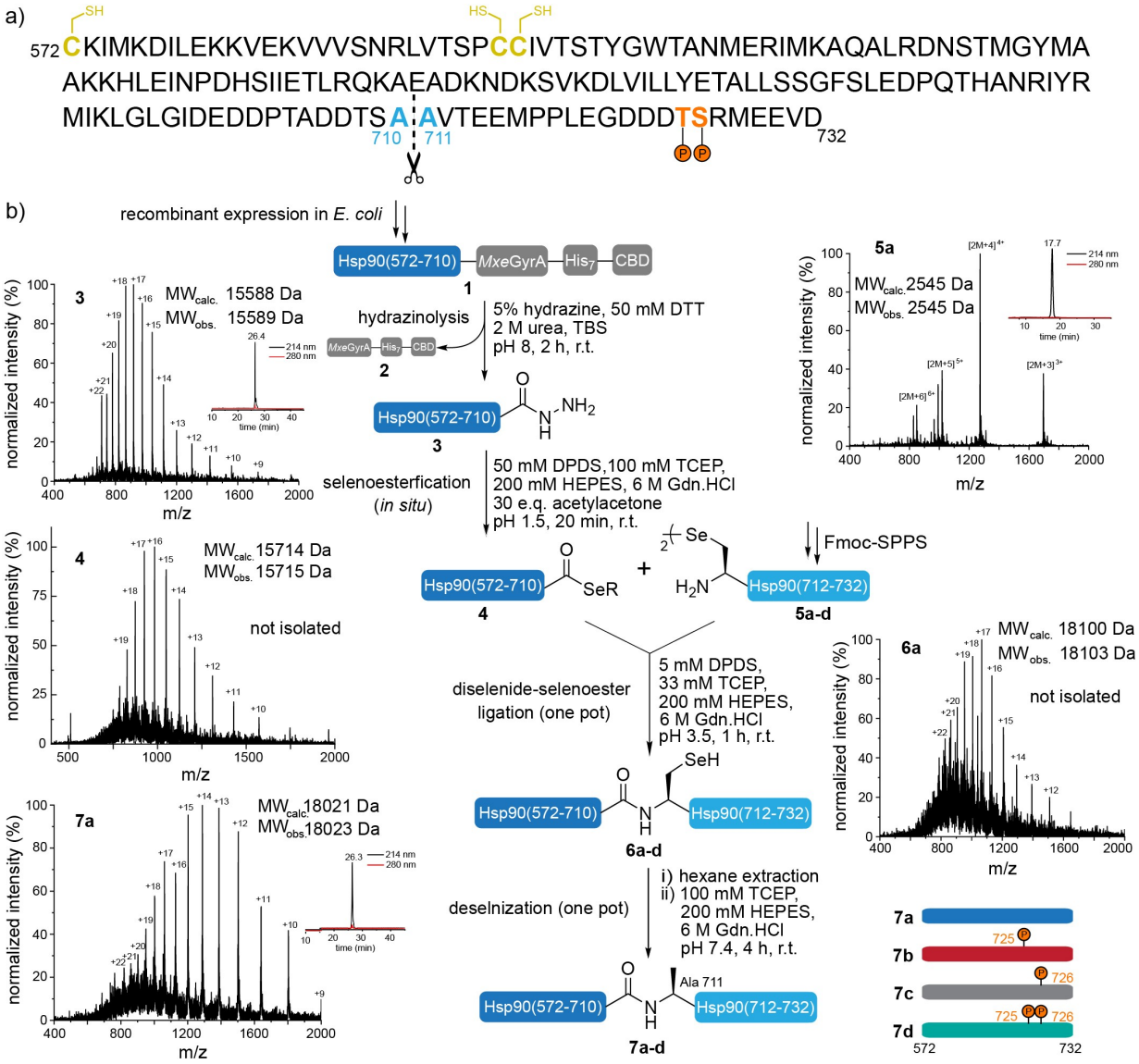

Figure 2. a) Sequence of Hsp90α CTD with native cysteine residues (yellow), ligation site (blue) and phosphorylation PTMs at the C-terminus (orange). b) Schematic overview of the semi-synthesis strategy for generation of site-selectively modified Hsp90 CTD *via* expressed protein selenoester ligation. Recombinant expression of segment 572-710 as intein-affinity tag fusion construct **1** yielded the desired hydrazide-functionalized segment **3** after intein **2** cleavage through hydrazinolysis. LC–MS monitoring confirmed the in situ selenoester conversion of segment **3**, which yielded the desired aryl selenoester **4** (not isolated). Modified and unmodified peptide segments 712–732 A711U (**5a–d**) were prepared by Fmoc-based SPPS. Successful ligation of **4** to synthetic peptides **5a–d** was confirmed *via* LC–MS and SDS-PAGE and yielded the desired ligation products **6a–d** (not isolated). After extraction of excess DPDS *via* hexane, TCEP-induced radical deselenization of **6a–d** was performed in a one-pot manner before RP-HPLC purification of the final deselenized products **7a–d**.

flexibility for further ligations to produce longer variants in future studies. The construct was expressed in the insoluble fraction inclusion bodies and the translation-initiating methionine was quantitatively cleaved by endogenous methionine aminopeptidase in *E. coli*. As is commonly observed for proteins bearing an N-terminal cysteine expressed in *E. coli*.,[43] the N-terminal cysteine reacted with the metabolite acetaldehyde forming a thiazolidine and resulting in an observed +24 Da mass increase (Supplementary Data Figure S1). After solubilization of the fusion protein from the inclusion bodies and purification, the intein-affinity tag **2** was cleaved *via* hydrazinolysis to yield the Hsp90_572-710 C-terminal hydrazide segment **3** after RP-HPLC purification. During the hydrazinolysis of the intein, the N-terminal thiazolidine was also cleaved, presumably due to excess hydrazine acting as a nucleophile and shifting the equilibrium away from the thiazolidine by reacting with the aldehyde. The resulting hydrazide segment **3** (Figure 2) therefore had the expected mass 15 588 Da.

Four variants **5a-d**, of the synthetic C-terminal segment (Hsp90_712-732) were synthesized using standard Fmoc-SPPS with *O*-benzyl side chain protected phospho-building blocks (Fmoc-Thr(PO(OBzl)OH)–OH/ Fmoc-Ser(PO(OBzl)OH)–OH). A 4-methoxybenzyl (Mob) protected selenocysteine was installed at the N-terminus instead of Ala711. After deprotection and purification, this yielded four Hsp90 CTD variants **5a**–**d** – unmodified **5a**, singly phosphorylated (pThr725, **5b** or pSer726, **5c**), and doubly phosphorylated **5d**, as diselenide dimers (Supplementary Figure S3).

Conversion of the Hsp90_572-710 C-terminal hydrazide segment **3** to the selenoester **4**, diselenide-selenoester ligation, and subsequent deselenization were carried out sequentially in one pot, taking advantage of the fast reaction kinetics of the diselenide-selenoester ligation and selectivity of deselenization, and avoiding the RP-HPLC purification of intermediates. Herein, the hydrazide segment **3** was converted cleanly to the respective aryl selenoester **4** using acetylacetone to form the active pyrazole intermediate, followed by diphenyldiselenide (DPDS) as selenol donor (Supplementary Figure S4). We continued by adding a slight excess (1.2 e.q.) of the respective synthetic Hsp90_712-732 segment **5a**–**d** dissolved in ligation buffer lacking TCEP to the freshly formed selenoester **4**, thereby diluting the TCEP to ~33 mM and suppressing premature deselenization of the selenocysteine through radical-mediated reduction by TCEP. Quantitative formation of the respective ligation products **6a-d** was observed in 30 minutes to 1 hour (Figure 2 and Supplementary Figure S5). Gratifyingly, we did not observe any ligation between the aryl selenoester and the unprotected N-terminal cysteine of the Hsp90_571-710 segment, either intra- or intermolecularly, and thereby avoided an additional thiol protection step to prevent cyclization or polymerization, respectively. This can be explained by the faster kinetics of the diselenide-selenoester ligation compared to a cysteine-selenoester ligation, due to the higher nucleophilicity of the selenolate compared to the corresponding thiolate.[35,44]

Proceeding with the deselenization of the ligation products **6a**–**d** in a one-pot manner, the excess free phenylselenol was removed *via* hexane extraction to prevent it acting as a radical quencher, and deselenization buffer was added (v/v 1:1, final TCEP concentration 100–150 mM) (Supplementary Figure S6). Initially the deselenization was sluggish, but after optimization of the reaction at pH 7.4, it proceeded with good conversion (70-80%) in four hours to yield the four semi-synthetic Hsp90_572-732 CTD variants **7a**–**d** (Supplementary Figure S7). In the presence of high TCEP concentrations (>100 mM), we observed that some undesired desulfurization of the native cysteines occurred if the reaction was left too long (>four hours). To avoid this, it was necessary to monitor the deselenization reaction carefully, and promptly freeze the reaction mixture at −80 °C on completion of the deselenization. After 1:1 dilution with 6 M Gdn.HCl, purification by RP-HPLC gave the isolated Hsp90 CTD variants **7a**–**d** in overall yields of 40–50% for the three steps carried on in one pot. Considering the hydrophobic nature of the Hsp90 CTD that causes significant losses for each RP-HPLC purification step, the optimization of the expressed protein selenoester ligation to carry out all three steps in one-pot represents an efficient strategy for generation of site-selectively modified Hsp90 CTD variants, and offers perspective for semi-synthesis of other hydrophobic proteins. Although selective deselenization has been demonstrated in the presence of internal cysteine residues, we believe this is the first report of deselenization in the presence of a free N-terminal cysteine residue, enabling subsequent ligations.

Impact of Phosphorylations on Secondary Structure and Thermal Stability

With the site-specifically phosphorylated Hsp90 CTD variants **7a**–**d** in hand, we investigated the effect of the phosphorylations on structure and stability. Due to the hydrophobicity of the CTD, direct dissolution of the lyophilized proteins in neutral buffers failed, so we carried out a re-folding step by dialysis from 6 M Gdn.HCl, TBS (50 mM Tris, 150 mM NaCl, 0.01% Tween20, pH 7.5) to the respective buffer for assays. Refolding was confirmed and overall secondary structure was determined by circular dichroism (CD) spectroscopy at a protein concentration of 0.2 mg/mL. CD spectra of the unmodified variant **7a** as well as the single and double modified variants **7b**–**d** showed characteristic spectra of α-helical proteins (Figure 3a), in accordance with the literature and the CD spectrum of the recombinantly expressed WT CTD (Supplementary Figures S8 and S9).[18] The minima at 207 nm and 225 nm for the doubly phosphorylated variant **7d** are slightly more intense than those for the unmodified and singly-modified variants **7a**–**c**, possibly indicating a slightly increased α-helical content. Whereas AlphaFold3[45] predictions suggest that the C-terminal tail of the CTD wraps around the CTD upon phosphorylation, the isolated synthetic Hsp90_711-732 variants all remained intrinsically disordered upon phosphorylation in solution NMR experiments (Supplementary Data Figure S10).

The thermal stabilities of the semi-synthetic CTD variants **7a**–**d** were compared using nano differential scanning fluorimetry (nanoDSF, Figure 3b), which uses the ratio of fluorescence intensities at 350 and 330 nm originating from intrinsic

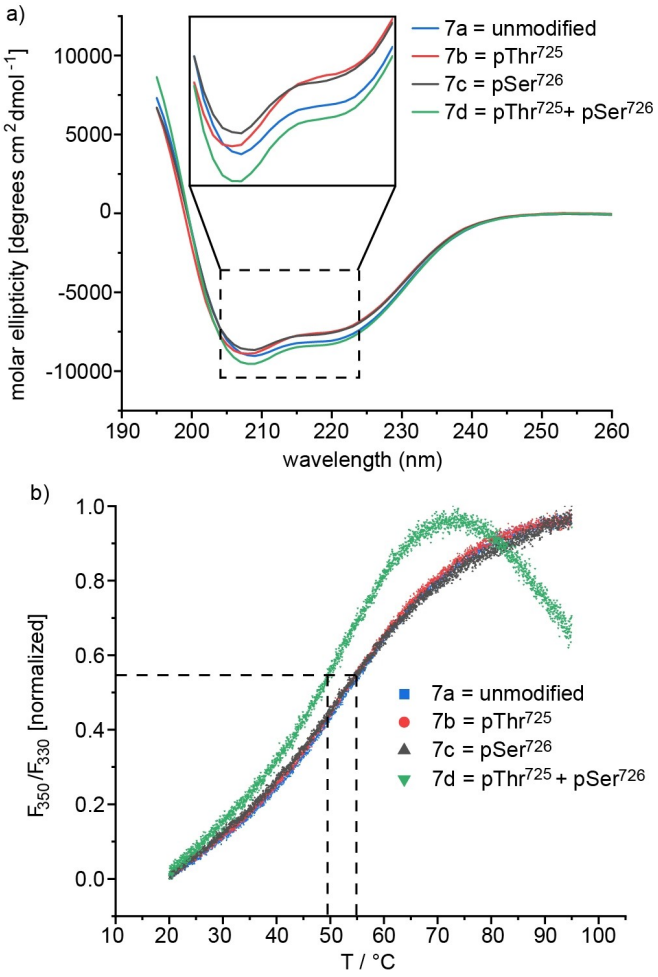

Figure 3. a) Structural characterization of CTD variants *via* circular dichroism (CD) spectroscopy with expanded alpha helical region between 205 and 225 nm (inset). CD spectra were measured in 50 mM KPO_4 buffer at pH 7.6 (protein concentration 0.2 mg/mL). b) Nano differential scanning fluorimetry of semi-synthetic Hsp90 CTD variants showing lower thermal stability of the doubly phosphorylated CTD variant **7 d** compared to the unmodified and singly modified variants **7 a**–**c**.

tryptophan or tyrosine fluorescence to monitor protein unfolding upon heating. NanoDSF experiments were carried out in the buffer used for refolding (NaP_i, pH 7.4), at which the Hsp90 CTD is reported to be thermally stable.[18] The low signal intensity, presumably caused by the presence of only one tryptophan (Trp606) and two tyrosine (Tyr 604 and Tyr689) residues in the CTD, prevented determination of precise melting temperature (Tm) values. Nevertheless, a difference in the melting behavior of the double modified variant **7 d** compared to the single modified and unmodified variants **7 a**–**c** is observable (Figure 3b, dotted lines), suggesting a lowering of the Tm value by ~3-5 °C upon double phosphorylation. The observed maximum of the F350/F330 ratio curve for **7 d** at ~70 degrees, followed by a decrease at higher temperatures, was interpreted to indicate unfolding followed by aggregation.

Phosphorylation at the C-Terminus Does Not Alter Hsp90 CTD Chaperone (Anti-Aggregation) Activity In-Vitro

The chaperone activities of the semi-synthetic Hsp90 CTD variants were compared, as previous studies in the literature have shown that the isolated CTD exhibits chaperone (anti-aggregation) capabilities in a variety of *in vitro* aggregation assays with model substrates.[17–19] We examined the anti-aggregation activities of our CTD variants using alcohol dehydrogenase (ADH) and insulin aggregation assays in which aggregation was monitored by an increase in absorption at 360 nm. Whereas aggregation of ADH was thermally induced by increasing the temperature to 55 °C, insulin aggregation was induced by reduction of the disulfide bonds by DTT. In both assays, all Hsp90 CTD variants displayed chaperone (anti-aggregation) activity; both the rate and extent (~60 % for ADH, ~55 % for insulin) of aggregation was decreased with respect to the controls (Figure 4). From the chaperone activities, we infer that the semi-synthetic Hsp90 CTD variants were refolded to form functional homodimers, as chaperone activity has been reported to correlate with dimer formation.[17] However, there were no significant differences between the activities of the four Hsp90 CTD variants **7 a-d**, leading us to conclude that neither of the two phosphorylations in the C-terminal tail has an impact on the chaperone (anti-aggregation) activity with these model substrates. More detailed binding studies with co-chaperones having the TPR domain are needed to determine if these phosphorylations affect recognition of the nearby -MEEVD region.

Conclusion

We demonstrate with the semi-synthesis of differently-phosphorylated Hsp90 CTD variants an application of the recently-reported expressed protein selenoester ligation that allows us to carry out both the ligation and deselenization steps in the presence of unprotected native cysteines, including an N-terminal cysteine. The latter provides an additional level of flexibility, as it allows potential N-terminal elongation of the obtained Hsp90 CTD by native chemical ligation. Furthermore, the optimized workflow and conditions to carry out the selenoesterification, diselenide-selenoester ligation and deselenization in one pot prevented the need for RP-HPLC purification of the intermediates, with associated loss of material. This allowed us to generate 3–6 mg amounts of each of the site-specifically modified Hsp90 CTD variants, and could be more broadly utilized for semi-synthesis of other hydrophobic proteins in the future. In further studies, the semi-synthesis strategy could also be applied to other PTMs in the CTD, and leaves the door open to extending the ligation strategy to the middle domain using the preserved N-terminal cysteine.

Despite successful refolding of the Hsp90 CTD variants and demonstration of their chaperone activity, the two phosphorylations in the C-terminal tail did not significantly affect the overall structure, or the chaperoning activity for the model substrates ADH and insulin. These results highlight the ongoing

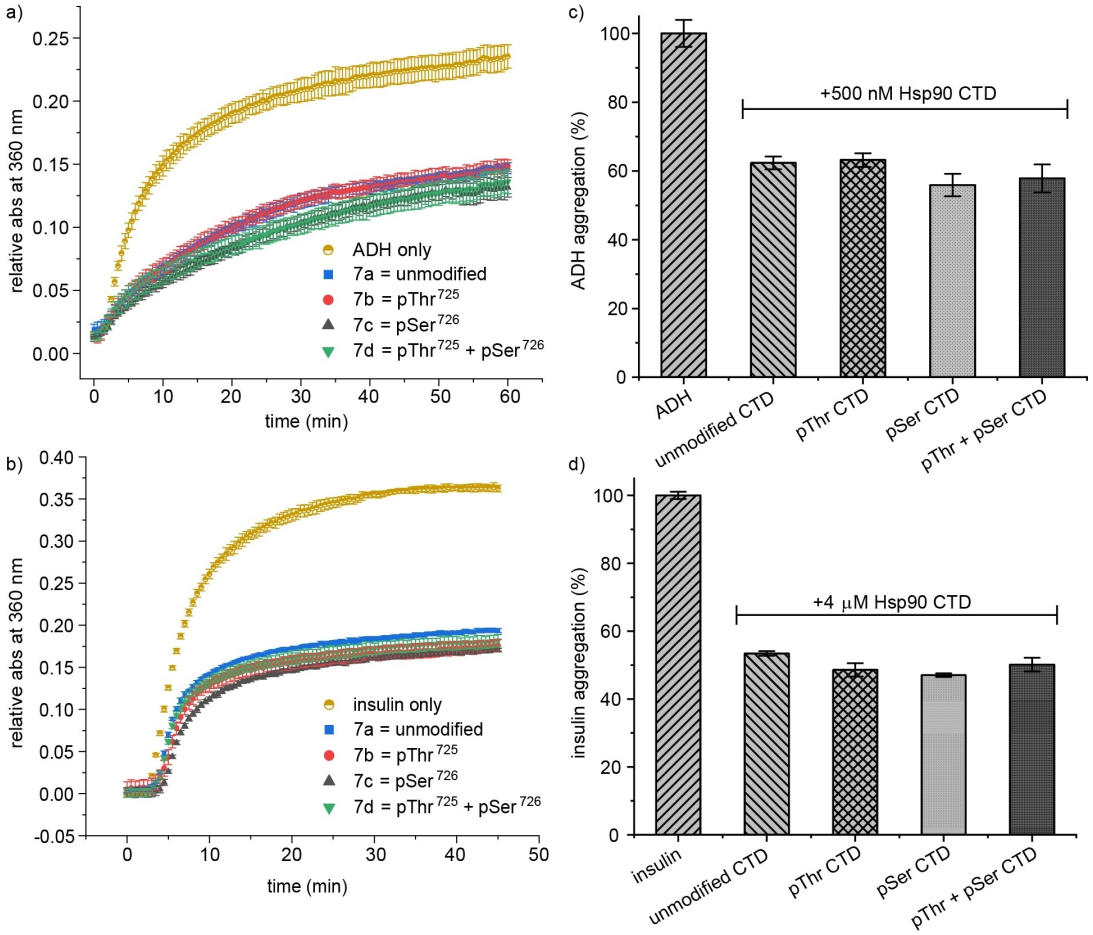

Figure 4. Chaperone activity in vitro of phosphorylated and unmodified Hsp90 CTD variants **7a–d** using ADH and insulin aggregation assays. a) ADH (3.1 μM) aggregation was induced by incubation at 55 °C in the presence and absence of 500 nM **7a–d** and monitored by measuring the absorbance at 360 nm over 60 min. Displayed are mean curves of triplicate measurements and error bars represent the standard deviation. b) Endpoint mean values (60 min) of ADH aggregation without addition of CTD were set to 100% and compared with mean values at 60 min from samples with Hsp90 CTD variants. Measurements were carried out in triplicate and error bars represent the standard deviation. c) Insulin (40 μM) aggregation was induced by addition of 20 mM DTT in the presence and absence of 4 μM **7a–d** and monitored by measuring the absorbance at 360 nm over 45 min at 37 °C (triplicate measurements). d) Endpoint mean values (45 min) of insulin aggregation (40 μM) without addition of CTD were set to 100% and compared with mean values at 45 min from samples with Hsp90 CTD variants (4 μM). Measurements were carried out in triplicate and error bars represent the standard deviation.

need to better understand the regulatory roles of PTMs in intrinsically disordered regions of proteins, and how these dynamic regions interact with the structured domains and with other protein binding partners. The two phosphorylations in the C-terminal tail increase the negative charge in an already highly negatively charged region, suggesting potential impacts on electrostatic interactions with positively charged regions, or possible metal coordination. Although pyrophosphorylation has been reported for Hsp90 (residues Ser255 and Ser263),[46] also in highly negatively charged regions, the proteomics data so far indicates that the PTMs on the C-terminal tail residues Thr725 and Ser726 are adjacent phosphorylations.[33] The location of the phosphorylations adjacent to the -MEEVD TRP sequence suggests that these PTMs might have a role in regulating Hsp90 by influencing the selection of co-chaperones, many of which are still not well understood. Access to site-specifically modified Hsp90 CTD variants now gives access to such studies, as well as the potential to explore the effects of mixed dimers bearing different PTMs in the chaperone code. Taken together, the complete elucidation of the Hsp90 chaperone code, which requires a detailed study of the individual impact of PTMs, their crosstalk and interplay with other proteins remains an enormous challenge, but is important to understand the complex biology of Hsp90 as a central regulator of cellular homeostasis.

Materials and Methods

Solid Phase Peptide Synthesis

Synthetic Hsp90 segments 711–732 (U711A) were prepared manually *via* 9-fluorenylmethoxycarbonyl (Fmoc) based solid phase peptide synthesis (SPPS) in 10 mL syringes equipped with a polypropylene filter on preloaded Tentagel resin (loading: 0.19 mmol/g). Fmoc-protected amino acid building blocks (2.5 equiv.) were double-coupled for 20–30 min at room temperature using *O*-(7-azabenzotriazol-1-yl)-*N,N,N′,N′*-tetramethyluronium-hexafluorphosphate (HATU, 2.4 equiv., 0.5 M in DMF) as activator and diisopropylethylamine (DIPEA, 5 equiv.) as base.

Fmoc-deprotection was achieved *via* incubation in 20% piperidine (3×3 min). Phosphorylated serine/threonine residues were introduced *via* Fmoc-protected Ser(PO(OBzl)OH)–OH or Thr(PO-(OBzl)OH)–OH (CEM) respectively and the N-terminal selenocysteine as Fmoc-L-Sec(Mob)–OH (Iris Biotech). The selenocysteine building block was double coupled using OxymaPure (0.5 M in DMF) and diisopropyl carbodiimide (DIC, 0.25 M in DMF) with a coupling time of 30–45 min. After final coupling and deprotection, peptides were washed with DCM and dried under vacuum overnight and cleaved from the resin with trifluoroacetic acid (TFA)/dimethyl disulfide (DMDS)/dimethyl sulfide (DMS)/ triisopropylsilane (TIPS)/H_2O 90:5:2.5:2.5 for 2.5 h followed by ether precipitation and pelleting *via* centrifugation (4000 g, 5 min). The crude peptide pellet was dissolved in acetonitrile/ water 1:1 and lyophilized prior to the final deprotection of the DMDS *trans* protected N-terminal selenocysteine *via* dissolving in 6 M guanidinium hydrochloride (Gdn.HCl), 20 mM DTT in ddH_20 for 30 min. The resulting diselenide peptide dimer was directly purified using RP-HPLC on a preparative scale C18 column (Kromasil) using a gradient of ACN in water with 0.1% TFA. Peptide purity was assessed *via* electrospray ionization mass spectrometry in positive ion mode and *via* analytical RP-HPLC.

Recombinant Expression and Purification of Hsp90 572-710-Hydrazide

For the generation of the recombinant segment Hsp90 572-710-hydrazide (**2**), a synthetic oligonucleotide comprising human Hsp90alpha 572-710-*Mxe* GyrA-His_7-CBD (sequence in Supplementary Data) was ordered from Eurofins Genomics in a pET-21a (+) vector and heat shock transformed into chemically competent *E.coli* strains XL1-Blue, BL21 (DE3) and Rosetta 2 (DE3) from Invitrogen. *E. coli* Rosetta 2(DE3) was used for expression and were grown in LB medium (10 g L^{-1} tryptone, 5 g L^{-1} yeast extract, 10 g L^{-1} NaCl) containing 100 μg mL^{-1} ampicillin and 30 μg mL^{-1} chloramphenicol. Overnight cultures were diluted to a starting OD of ~0.2, and were grown at 37 °C with shaking at 170 rpm to an OD of 0.7-0.8 before induction of expression with 1 mM IPTG. After 4 h at 37 °C (170 rpm), cells were harvested *via* centrifugation (12000 g, 20 min) and cell pellets stored at −80 °C before further workup. After thawing, 1 × TBS buffer (50 mM Tris, 150 mM NaCl, 0.01% Tween20, pH 7.5) was added to the cell pellet (50 mL buffer / 1 L expression pellet) and the solution homogenized using an ultra turax before cell lysis *via* sonification on ice (60% amplitude, 15 sec ON, 45 sec OFF time, total ON time 10 min). After clearing the supernatant *via* centrifugation (21000 rpm, 53000 g, 45 min at 4 °C), the collected inclusion bodies were solubilized by incubation in 6 M Gdn.HCl, TBS buffer at pH 7.5 while stirring overnight at r.t.. After removal of insoluble cell debris (21000 rpm, 53000 g, 45 min), the solution was directly dialyzed against 4 M Urea, TBS pH 8 at 4 °C overnight before inducing intein-mediated hydrazinolysis *via* dropwise addition of 10% hydrazine, 100 mM DTT in TBS pH 8 (1:1 dilution) (final concentration: 5% Hydrazine, 50 mM DTT, 2 M urea in TBS). After 2 h, the solution was diluted further 1:1 with 6 M Gdn.HCl, filtered and purified *via* RP-HPLC on a preparative scale C4 column (Kromasil) with a gradient of 30–60% ACN in water (+0.1% TFA) at a flow rate of 10 mL/min at 60 °C. Peak fractions were pooled and lyophilized yielding compound **2** at ~10 mg/L culture.

Selenoester Formation, Diselenide-Selenoester Ligation and Deselenization

The purified and lyophilized recombinant segment **2** was dissolved in freshly prepared and degassed 6 M Gdn.HCl, 100 mM TCEP, 50 mM DPDS, 200 mM HEPES buffer at a concentration of 1–1.3 mM and the pH adjusted to 1.5. Selenoester formation was initiated by the addition of ~30 equiv. acetylacetone and the reaction monitored *via* electrospray ionization mass 15–30 min. Synthetic peptide variants Hsp90 **5a–d** were dissolved in 6 M Gdn.HCl, 5 mM DPDS, 200 mM HEPES buffer (1.5 equiv. based on recombinant segment) and directly added to Hsp90 (572-710)-SeR *via* 1:2 dilution (final TCEP concentration in the ligation mixture 33 mM) after successful selenoester formation was confirmed *via* ESI-MS. The pH was adjusted to 3.5-4 using NaOH and the Eppendorf tube flushed with argon before incubation of the reaction mixture at r.t. with stirring. The ligation reaction was monitored *via* ESI-MS and SDS-PAGE, and after 1 h, excess phenylselenol (DPDS) was removed *via* hexane extraction (5 ×, 1:1 vol/vol) before continuing with the deselenization. Deselenization was performed by diluting the reaction mixture 1:1 with freshly prepared and degassed deselenization buffer (6 M Gdn.HCl, 250 mM TCEP, 200 mM HEPES, 25 mM DTT). The pH was adjusted to 7.4 and the reaction was stirred at r.t. for 4–5 h under argon before being frozen at −80 °C. After thawing and dilution with 6 M Gdn.HCl in ddH_2O, the ligation product was purified on a semipreparative scale C4 column (Kromasil) using a linear gradient from 30–65% of solvent B (ACN + 0.08% TFA) in solvent A (ddH_2O + 0.1% TFA) at a flow rate of 5 mL/min at 60 °C. Fractions containing the deselenized ligation product were analysed by ESI-MS, combined and lyophilized. Final yields of lyophilized ligation products ranged between 45–50% based on segment **2** as limiting starting material.

Recombinant Expression and Purification of Full Length Hsp90 CTD

The synthetic oligonucleotide comprising N-terminally His_6-tagged human Hsp90alpha CTD (sequence in Supplementary Data) was ordered from Eurofins Genomics in a pET-21a (+) vector and heat shock transformed into chemically competent *E.coli* strains XL1-Blue, BL21 (DE3) and Rosetta 2 (DE3) from Invitrogen. Expression using *E. coli* Rosetta 2(DE3) strain and subsequent cell lysis was performed analogously to the fusion construct **1**. After cell lysis and separation of cell debris *via* centrifugation (21000 rpm, 53000 g, 45 min at 4 °C), the cleared supernatant which contained the soluble fraction of the overexpressed protein was loaded onto a preequilibrated Ni-NTA resin on an Äkta Prime FPLC system. The protein was eluted using a gradient of 25–500 mM imidazole and the fractions analyzed using SDS-PAGE (Supplementary Figure S8b). Pooled fractions were further purified *via* RP-HPLC on a preparative scale C4 column (Kromasil) with a gradient of 30–75% ACN in water (+0.1% TFA) in 40 min at a flow rate of 10 mL/min at 60 °C. Peak fractions were combined and lyophilized yielding the desired protein at ~15 mg/L culture Supplementary Figure S8c).

Protein Refolding and Circular Dichroism Spectroscopy

Lyophilized semi-synthetic Hsp90 variants and recombinant WT CTD were dissolved in 6 M Gdn.HCl TBS buffer and dialyzed towards assay buffer (50 mM KPO_4 buffer pH 7.6) at 4 °C overnight. Circular dichroism spectroscopy was performed in 50 mM KPO_4 buffer pH 7.6 at a protein concentration of 0.2 mg/mL using an JASCO J-815/150S spectropolarimeter at 20 °C and a path length of 1 mm. Scans were recorded in the range of 195 to 260 nm and the shown spectra are the average of five measurements after signal correction *via* buffer subtraction.

Thermal Stability Determination by Nano Differential Scanning Fluorimetry

Thermal stability assessments were performed using a Prometheus NT.48 (Nanotemper) in 50 mM NaPi, 150 mM NaCl pH 7.5 buffer at

2 mg/mL protein concentration. Protein denaturation was monitored by measuring the ratio of the tryptophan fluorescence intensities at 350 nm and 330 nm while increasing the temperature from 20 to 95 °C at 1 °C/ min. Triplicates were measured, averaged, and corrected *via* buffer subtraction. Depicted curves are normalized between values 0.0 and 1.0 for better visual comparison.

Aggregation Assays

The anti-aggregation (chaperoning) capabilities of Hsp90 variants **7a-d** were measured using an alcohol dehydrogenase (ADH) and insulin aggregation assay similar to previously reported methods.[18,47] Equine ADH (Sigma) was directly dissolved in assay buffer (50 mM NaPi, 100 mM NaCl pH 7.0) and the concentration determined *via* BCA assay before dilution to the assay concentration (3.1 μM). CTD variants **7a–d** were dialyzed towards assay buffer, the concentration determined (BCA) and added to ADH to a final concentration of 500 nM (final volume 1400 μL). ADH aggregation was thermally induced at 55 °C and monitored over 60 min by measuring the absorbance at 360 nm in a SAFAS UVmc2 spectrophotometer equipped with a temperature-controlled multicell holder (SAFAS, Monaco) in 700 μL quartz cuvettes (Hellma Analytics). Samples were measured as triplicates and the end point of ADH aggregation readout set to 100% to compare chaperoning efficiency. For determination of insulin aggregation inhibition bovine pancreas insulin (Sigma) was dissolved in 1% acetic acid in ddH_2O and the stock concentration determined using a NanoDrop 2000 (molar extinction coefficient used: 5,734 $cm^{-1}M^{-1}$). The insulin stock was diluted to 40 μM using assay buffer (50 mM NaPi, 100 mM NaCl pH 7.4), prior to the addition of Hsp90 CTD variants **7a–d** (4 μM) dialyzed into the assay buffer. The protein solution was incubated for 15 min at r.t. before insulin aggregation was induced by the addition of 20 mM DTT. Insulin aggregation was measured by monitoring the absorbance at 360 nm in a SAFAS UVmc2 spectrophotometer equipped with a temperature-controlled multicell holder (SAFAS, Monaco) in 700 μL quartz cuvettes (Hellma Analytics) for 45 minutes. Triplicates were measured, baseline subtracted and averaged and the end point of insulin aggregation set to 100% for the comparison of chaperoning efficiency.

Acknowledgements

This project was partly supported by an Australian Research Council Discovery Project (DP220101037) to A. C. Conibear and R. J. Payne.

O. Gajsek gratefully acknowledges funding from the Austrian Academy of Sciences (ÖAW) through a Doc.Fellowship (26072).

CD spectroscopy was supported by an Innovative Project (RAKI-MINT) granted by Vienna University of Technology to Astrid R. Mach-Aigner (Institute of Bioprocess Technologies, TU Wien).

The authors acknowledge TU Wien Bibliothek for financial support through its Open Access Funding Programme.

Conflict of Interests

The authors declare no conflict of interest.

Data Availability Statement

The data that support the findings of this study are available in the supplementary material of this article.

Keywords: Chaperones · Expressed Protein Selenoester Ligation · Hsp90 · Posttranslational modifications · Protein synthesis

[1] V. Dahiya, J. Buchner, *Adv. Protein Chem. Struct. Biol.* **2019**, *114*, 1–60, DOI: 10.1016/bs.apcsb.2018.10.001.
[2] G. G. Jayaraj, M. S. Hipp, F. U. Hartl, *Cold Spring Harbor Perspect. Biol.* **2020**, *12* (1), DOI: 10.1101/cshperspect.a033951.
[3] B. Chen, W. H. Piel, L. Gui, E. Bruford, A. Monteiro, *Genomics* **2005**, *86* (6), 627–637, DOI: 10.1016/j.ygeno.2005.08.012.
[4] F. H. Schopf, M. M. Biebl, J. Buchner, *Nat. Rev. Mol. Cell Biol.* **2017**, *18* (6), 345–360, DOI: 10.1038/nrm.2017.20.
[5] M. M. Biebl, J. Buchner, *Cold Spring Harbor Perspect. Biol.* **2019**, *11* (9), DOI: 10.1101/cshperspect.a034017.
[6] A. Hoter, M. E. El-Sabban, H. Y. Naim, *Int. J. Mol. Sci.* **2018**, *19* (9), DOI: 10.3390/ijms19092560.
[7] M. Radli, S. G. D. Rüdiger, *J. Mol. Biol.* **2018**, *430 (18, Part B)*, 3029–3040, DOI: 10.1016/j.jmb.2018.05.026.
[8] S. Weickert, M. Wawrzyniuk, L. H. John, S. G. D. Rudiger, M. Drescher, *Sci. Adv.* **2020**, *6* (11), eaax6999, DOI: 10.1126/sciadv.aax6999.
[9] L. M. Ramirez, M. Zweckstetter, *Curr. Opin. Chem. Biol.* **2023**, *74*, 102304, DOI: 10.1016/j.cbpa.2023.102304.
[10] X. Ren, T. Li, W. Zhang, X. Yang, *Cells* **2022**, *11* (16), DOI: 10.3390/cells11162556.
[11] J. Liu, H. Shu, Q. Xia, Q. You, L. Wang, *Expert Opin. Ther. Pat.* **2024**, *34 (1-2)*, 1–15, DOI: 10.1080/13543776.2024.2327295.
[12] T. S. Reynolds, B. S. J. Blagg, *Eur. J. Med. Chem.* **2024**, *277*, 116736, DOI: 10.1016/j.ejmech.2024.116736.
[13] T. Doi, N. Yamamoto, S. Ohkubo, *Future Oncol.* **2024**, *20* (9), 507–519, DOI: 10.2217/fon-2022-1172.
[14] K. Richter, P. Muschler, O. Hainzl, J. Buchner, *J. Biol. Chem.* **2001**, *276* (36), 33689–33696, DOI: 10.1074/jbc.M103832200.
[15] H. Zhang, C. Zhou, W. Chen, Y. Xu, Y. Shi, Y. Wen, N. Zhang, *Sci. Rep.* **2015**, *5* (1), 9542, DOI: 10.1038/srep09542.
[16] K. Tych, M. Jahn, H. Girstmair, T. Hugel, J. Buchner, M. Rief, *Biophys. J.* **2020**, *118 (3, Supplement 1)*, 198a, DOI: 10.1016/j.bpj.2019.11.1194.
[17] R. K. Allan, D. Mok, B. K. Ward, T. Ratajczak, *J. Biol. Chem.* **2006**, *281* (11), 7161–7171, DOI: 10.1074/jbc.M512406200.
[18] E. Ciglia, J. Vergin, S. Reimann, S. H. J. Smits, L. Schmitt, G. Groth, H. Gohlke, *PLoS One* **2014**, *9* (4), e96031, DOI: 10.1371/journal.pone.0096031.
[19] K. M. Goode, D. P. Petrov, R. E. Vickman, S. A. Crist, P. E. Pascuzzi, T. L. Ratliff, V. J. Davisson, T. R. Hazbun, *Biochim. Biophys. Acta Gen. Subj.* **2017**, *1861* (8), 1992–2006, DOI: 10.1016/j.bbagen.2017.05.006.
[20] J. C. Young, W. M. Obermann, F. U. Hartl, *J. Biol. Chem.* **1998**, *273* (29), 18007–18010, DOI: 10.1074/jbc.273.29.18007.
[21] V. A. Assimon, D. R. Southworth, J. E. Gestwicki, *Biochemistry* **2015**, *54* (48), 7120–7131, DOI: 10.1021/acs.biochem.5b00801.
[22] K. L. Blundell, M. Pal, S. M. Roe, L. H. Pearl, C. Prodromou, *PLoS One* **2017**, *12* (3), e0173543, DOI: 10.1371/journal.pone.0173543.
[23] S. J. Backe, R. A. Sager, M. R. Woodford, A. M. Makedon, M. Mollapour, *J. Biol. Chem.* **2020**, *295* (32), 11099–11117, DOI: 10.1074/jbc.REV120.011833.
[24] M. Mollapour, L. Neckers, *Biochim. Biophys. Acta.* **2012**, *1823* (3), 648–655, DOI: 10.1016/j.bbamcr.2011.07.018.
[25] A. Walton-Diaz, S. Khan, D. Bourboulia, J. B. Trepel, L. Neckers, M. Mollapour, *Future Med. Chem.* **2013**, *5* (9), 1059–1071, DOI: 10.4155/fmc.13.88.
[26] A. C. Conibear, *Nat. Chem. Rev.* **2020**, *4* (12), 674–695, DOI: 10.1038/s41570-020-00223-8.
[27] R. E. Thompson, T. W. Muir, *Chem. Rev.* **2020**, *120* (6), 3051–3126, DOI: 10.1021/acs.chemrev.9b00450.
[28] S. J. Backe, J. A. Heritz, M. Mollapour, *Autophagy* **2024**, *20* (7), 1689–1691, DOI: 10.1080/15548627.2024.2323259.

[29] S. J. Backe, R. A. Sager, J. A. Heritz, L. A. Wengert, K. A. Meluni, X. Aran-Guiu, B. Panaretou, M. R. Woodford, C. Prodromou, D. Bourboulia, *Cell Rep.* **2023**, *42* (7), 112807, DOI: 10.1016/j.celrep.2023.112807.
[30] P. Muller, E. Ruckova, P. Halada, P. J. Coates, R. Hrstka, D. P. Lane, B. Vojtesek, *Oncogene* **2013**, *32* (25), 3101–3110, DOI: 10.1038/onc.2012.314.
[31] D. Somale, G. Di Nardo, L. di Blasio, A. Puliafito, M. Vara-Messler, G. Chiaverina, M. Palmiero, V. Monica, G. Gilardi, L. Primo, *Sci. Rep.* **2020**, *10* (1), 591, DOI: 10.1038/s41598-019-56937-3.
[32] A. K. Pandey, H. K. Ganguly, S. K. Sinha, K. E. Daniels, G. P. A. Yap, S. Patel, N. J. Zondlo, *ACS Chem. Biol.* **2023**, *18* (9), 1938–1958, DOI: 10.1021/acschembio.3c00068.
[33] D. Ochoa, A. F. Jarnuczak, C. Viéitez, M. Gehre, M. Soucheray, A. Mateus, A. A. Kleefeldt, A. Hill, L. Garcia-Alonso, F. Stein, *Nat. Biotechnol.* **2020**, *38* (3), 365–373, DOI: 10.1038/s41587-019-0344-3.
[34] S. S. Kulkarni, E. E. Watson, B. Premdjee, K. W. Conde-Frieboes, R. J. Payne, *Nat. Protoc.* **2019**, *14* (7), 2229–2257, DOI: 10.1038/s41596-019-0180-4.
[35] S. S. Kulkarni, E. E. Watson, J. W. C. Maxwell, G. Niederacher, J. Johansen-Leete, S. Huhmann, S. Mukherjee, A. R. Norman, J. Kriegesmann, C. F. W. Becker, *Angew. Chem. Int. Ed. Engl.* **2022**, *61* (20), e202200163, DOI: 10.1002/anie.202200163.
[36] T. W. Muir, D. Sondhi, P. A. Cole, *Proc. Natl. Acad. Sci. USA* **1998**, *95* (12), 6705–6710, DOI: 10.1073/pnas.95.12.6705.
[37] Q. Wan, S. J. Danishefsky, *Angew. Chem. Int. Ed. Engl.* **2007**, *46* (48), 9248–9252, DOI: 10.1002/anie.200704195.
[38] N. Metanis, E. Keinan, P. E. Dawson, *Angew. Chem. Int. Ed. Engl.* **2010**, *49* (39), 7049–7053, DOI: 10.1002/anie.201001900.
[39] C. C. Lee, T. W. Lin, T. P. Ko, A. H. Wang, *PLoS One* **2011**, *6* (5), e19961, DOI: 10.1371/journal.pone.0019961.
[40] C. M. Noddings, R. Y. Wang, J. L. Johnson, D. A. Agard, *Nature* **2022**, *601* (7893), 465–469, DOI: 10.1038/s41586-021-04236-1.
[41] S. Peng, R. L. Matts, J. Deng, *J. Biomol. Struct. Dyn.* **2023**, *41* (19), 9745–9755, DOI: 10.1080/07391102.2022.2146197.
[42] N. J. Mitchell, S. S. Kulkarni, L. R. Malins, S. Wang, R. J. Payne, *Chemistry* **2017**, *23* (4), 946–952, DOI: 10.1002/chem.201604709.
[43] I. E. Gentle, D. P. De Souza, M. Baca, *Bioconjugate Chem.* **2004**, *15* (3), 658–663, DOI: 10.1021/bc049965o.
[44] A. C. Conibear, E. E. Watson, R. J. Payne, C. F. W. Becker, *Chem. Soc. Rev.* **2018**, *47* (24), 9046–9068, DOI: 10.1039/c8cs00573g.
[45] J. Abramson, J. Adler, J. Dunger, R. Evans, T. Green, A. Pritzel, O. Ronneberger, L. Willmore, A. J. Ballard, J. Bambrick, *Nature* **2024**, *630* (8016), 493–500, DOI: 10.1038/s41586-024-07487-w.
[46] J. A. M. Morgan, A. Singh, L. Kurz, M. Nadler-Holly, M. Ruwolt, S. Ganguli, S. Sharma, M. Penkert, E. Krause, F. Liu, *Nat. Chem. Biol.* **2024**, *20* (10), 1305–1316, DOI: 10.1038/s41589-024-01613-5.
[47] E. V. Mymrikov, M. Daake, B. Richter, M. Haslbeck, J. Buchner, *J. Biol. Chem.* **2017**, *292* (2), 672–684, DOI: 10.1074/jbc.M116.760413.

Manuscript received: October 3, 2024
Accepted manuscript online: November 14, 2024
Version of record online: ■■, ■■

RESEARCH ARTICLE

Expressed Protein Selenoester Ligation (EPSL) allows for an efficient generation of semi-synthetic Hsp90 CTD bearing site-specific phosphorylations in a traceless manner to facilitate elucidation of the chaperone code.

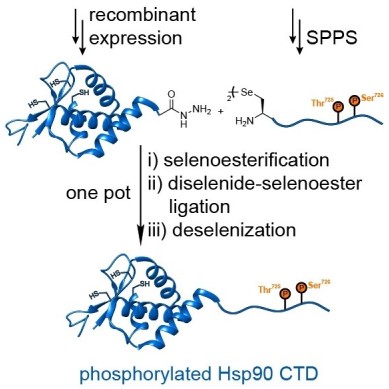

O. Gajsek, C. F. W. Becker, A. C. Conibear**